Title

Coercive Fields Exceeding 30 T in the Mixed-Valence Single-Molecule Magnet (CpiPr5)2Ho2I3.

Journal

Journal of the American Chemical Society, 146(27)

Authors

Kwon, Hyunchul

McClain, K

Kragskow, Jon

et al.

Publication Date

2024-07-10

DOI

10.1021/jacs.4c06250

Peer reviewed

JACS
JOURNAL OF THE AMERICAN CHEMICAL SOCIETY
pubs.acs.org/JACS

Article

Coercive Fields Exceeding 30 T in the Mixed-Valence Single-Molecule Magnet $(Cp^{iPr5})_2Ho_2I_3$

Hyunchul Kwon,◆ K. Randall McClain,*,◆ Jon G. C. Kragskow, Jakob K. Staab, Mykhaylo Ozerov, Katie R. Meihaus, Benjamin G. Harvey, Eun Sang Choi,* Nicholas F. Chilton,* and Jeffrey R. Long*

Cite This: J. Am. Chem. Soc. 2024, 146, 18714−18721

Read Online

ACCESS | Metrics & More | Article Recommendations | Supporting Information

ABSTRACT: Mixed-valence dilanthanide complexes of the type $(Cp^{iPr5})_2Ln_2I_3$ (Cp^{iPr5} = pentaisopropylcyclopentadienyl; Ln = Gd, Tb, Dy) featuring a direct Ln−Ln σ-bonding interaction have been shown to exhibit well-isolated high-spin ground states and, in the case of the Tb and Dy variants, a strong axial magnetic anisotropy that gives rise to a large magnetic coercivity. Here, we report the synthesis and characterization of two new mixed-valence dilanthanide compounds in this series, $(Cp^{iPr5})_2Ln_2I_3$ (**1-Ln**; Ln = Ho, Er). Both compounds feature a Ln−Ln bonding interaction, the first such interaction in any molecular compounds of Ho or Er. Like the Tb and Dy congeners, both complexes exhibit high-spin ground states arising from strong spin−spin coupling between the lanthanide 4f electrons and a single σ-type lanthanide−lanthanide bonding electron. Beyond these similarities, however, the magnetic properties of the two compounds diverge. In particular, **1-Er** does not exhibit observable magnetic blocking or slow magnetic relaxation, while **1-Ho** exhibits magnetic blocking below 28 K, which is the highest temperature among Ho-based single-molecule magnets, and a spin reversal barrier of 556(4) cm^{-1}. Additionally, variable-field magnetization data collected for **1-Ho** reveal a coercive field of greater than 32 T below 8 K, more than 6-fold higher than observed for the bulk magnets $SmCo_5$ and $Nd_2Fe_{14}B$, and the highest coercive field reported to date for any single-molecule magnet or molecule-based magnetic material. Multiconfigurational calculations, supported by far-infrared magnetospectroscopy data, reveal that the stark differences in magnetic properties of **1-Ho** and **1-Er** arise from differences in the local magnetic anisotropy of the lanthanide centers.

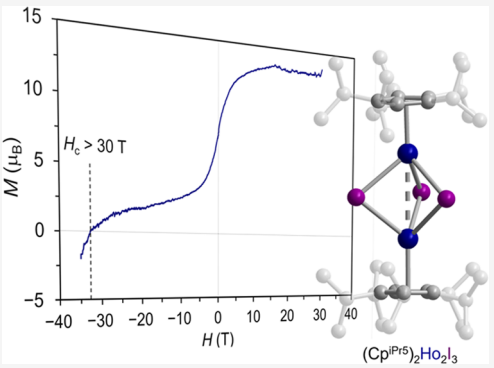

INTRODUCTION

For the last three decades, the lanthanide elements have played a key role in advancing the field of single-molecule magnets, which have potential applications in the quantum sciences and high-density information storage.[1,2] The trivalent lanthanides are particularly well-suited for the design of single-molecule magnets, owing to their large single-ion anisotropies, which arise from the unquenched orbital angular momentum of the core-like 4f orbitals.[3,4] Judicious design of the electrostatic crystal field for a given lanthanide ion has been one of the most promising strategies to date for the design of mononuclear single-molecule magnets,[5] in many cases giving rise to systems that exhibit magnetic blocking near liquid nitrogen temperatures.[6,7] In general, an axial ligand field can be used to stabilize the oblate electron density associated with the maximal M_J states of lanthanide ions such as Tb^{III} and Dy^{III}, whereas an equatorial crystal field stabilizes the prolate electron density associated with the largest M_J states of ions such as Er^{III}.[8,9] The series of mononuclear Dy^{III} metallocene compounds of the type $[Dy(Cp^R)_2]^+$ (Cp^R = substituted cyclopentadienyl) well exemplifies this approach: the two Cp^R ligands provide a strong axial crystal field, and molecules in this class exhibit magnetic blocking temperatures (T_b, defined here as the temperature at which the magnetic relaxation time is 100 s) above 50 K.[10]

While the trivalent lanthanides have long dominated the field, the discovery of divalent lanthanide ions with $4f^n5d^1$ electronic configurations[11−14] has expanded the design toolkit for single-molecule magnets. For example, reduction of the bent metallocene complex $[Tb(Cp^{iPr5})_2]^+$ (Cp^{iPr5} = pentaisopropylcyclopentadienyl) yields $Tb(Cp^{iPr5})_2$, which features a half-integer spin Kramers ion Tb^{II} and a perfectly linear Cp−Tb−Cp angle.[15] As a result, the magnetic relaxation times for $Tb(Cp^{iPr5})_2$ are significantly longer than those of $[Tb(Cp^{iPr5})]^+$, and $Tb(Cp^{iPr5})_2$ exhibits a record blocking temperature of T_b = 52 K for a mononuclear, nondysprosium single-molecule magnet. Exploiting this $4f^n5d^1$ electronic configuration, some of us have also recently reported the first mixed-valence lanthanide complexes $(Cp^{iPr5})_2Ln_2I_3$ (Ln =

Received: May 9, 2024
Revised: June 12, 2024
Accepted: June 12, 2024
Published: June 26, 2024

https://doi.org/10.1021/jacs.4c06250
J. Am. Chem. Soc. 2024, 146, 18714−18721

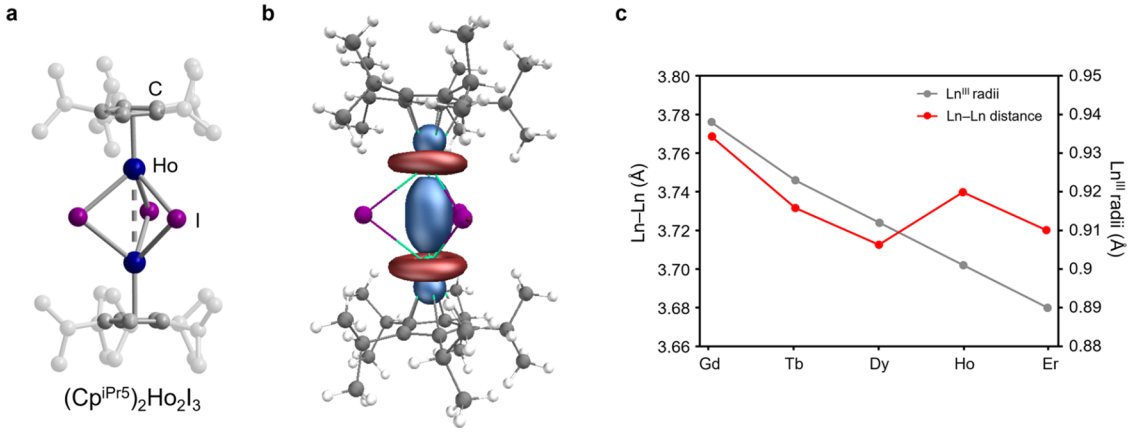

Figure 1. (a) Structure of **1-Ho**, as obtained from a single-crystal X-ray diffraction analysis (see Figure S8 for the structure of **1-Er**). Dark blue, purple, and gray spheres represent Ho, I, and C atoms, respectively; H atoms have been omitted for clarity. Selected interatomic distances for **1-Ho** and **1-Er**, respectively: Ln−Ln = 3.740(1), 3.720(1) Å; Ln−Cp(cent) = 2.333(1), 2.313(1) Å. (b) Illustration of the σ-bonding SOMO for **1-Ho** obtained from CASSCF-SO calculations. (c) Plot of the Ln−Ln distances in **1-Ln** for Ln = Gd, Tb, Dy, Ho, Er (left axis), along with the corresponding Ln^{III} radii (right axis).[17]

Y, Gd, Tb, Dy), prepared via one-electron reduction of the trivalent complexes $(Cp^{iPr5})_2Ln_2I_4$.[16] These compounds exhibit valence delocalization due to the formation of a singly occupied σ-bonding molecular orbital of $5d_{z^2}$ parentage. Multiconfigurational complete active space self-consistent field (CASSCF) calculations carried out on the Tb and Dy variants revealed that the axial ligand field afforded by the Cp^{iPr5} ligands and the σ electron serves to stabilize the maximal total $|M_J|$ ground state for these compounds.[16] In tandem with strong spin−spin coupling between the 4f electrons and the σ electron, this electronic structure gives rise to well-isolated, large total angular momentum ground states, large barriers to slow magnetic relaxation, and in the case of $(Cp^{iPr5})_2Dy_2I_3$, a record blocking temperature of T_b = 72 K and the largest coercive magnetic field (H_c) reported to date for any molecule-based magnetic material.

Here, we present two new mixed-valence dilanthanide complexes in this family, $(Cp^{iPr5})_2Ln_2I_3$ (**1-Ln**; Ln = Ho, Er). Detailed magnetic, computational, and spectroscopic analyses reveal that, while both compounds exhibit strong 4f−σ spin−spin coupling, the axial crystal field has a dramatically different effect on their electronic structures. In the case of **1-Er**, the axial crystal field destabilizes the prolate maximal M_J levels of the individual Er^{III} centers, such that the compound does not behave as a single-molecule magnet. In contrast, for **1-Ho**, which features Ho^{III} centers with maximal M_J states that are more oblate in character, the crystal field stabilizes the maximal possible total $|M_J|$ ground state. As a result, this compound exhibits a record blocking temperature among holmium single-molecule magnets and a magnetic coercivity of 32.6 T—the largest reported to date for any single-molecule magnet or molecule-based magnetic material.

RESULTS AND DISCUSSION

Synthesis and Characterization. The compounds **1-Ho** and **1-Er** were synthesized following the previously reported route to $(Cp^{iPr5})_2Ln_2I_3$ (Ln = Y, Gd, Tb, Dy).[16] In brief, the trivalent dilanthanide complexes $(Cp^{iPr5})_2Ln_2I_4$ (Ln = Ho, Er) were synthesized via high-temperature salt metathesis between LnI_3 and one equivalent of $NaCp^{iPr5}$ in toluene. After filtration, solvent removal, and washing with pentane, $(Cp^{iPr5})_2Ho_2I_4$ and $(Cp^{iPr5})_2Er_2I_4$ were isolated as analytically pure yellow or pink powders, respectively. Reduction of $(Cp^{iPr5})_2Ln_2I_4$ (Ln = Ho, Er) with excess KC_8 in *n*-hexane resulted in the formation of dark green-blue (Ho) or green (Er) solutions after several days. These solutions were filtered to remove KI and unreacted KC_8, concentrated, and stored at −35 °C. Analytically pure prismatic green-blue (**1-Ho**) or brown-green (**1-Er**) single crystals suitable for X-ray diffraction analysis were isolated after several days. The crystals were found to be indefinitely stable at room temperature under argon, although at ambient temperature in the presence of air and moisture, they decayed rapidly, forming yellow or colorless solids. The compounds are stable in pentane and hexane or electron-rich arene solvents such as 1,3,5-trimethylbenzene, but they decompose in benzene or toluene over the course of several minutes.

The solid-state structures of **1-Ho** and **1-Er** were obtained by single-crystal X-ray diffraction analyses (Figures 1a, S6, and S8). Both structures feature an Ln_2I_3 core with two crystallographically equivalent lanthanide ions connected by three bridging iodide ligands and capped with a $(Cp^{iPr5})^-$ ligand. The Ln···Ln distances in **1-Ho** and **1-Er** are 3.740(1) and 3.720(1) Å, respectively, within the range of those previously reported for $(Cp^{iPr5})_2Ln_2I_3$ (Ln = Y, Gd, Tb, Dy).[16] From these values, we calculated a formal shortness ratio for each compound—defined as the ratio of the experimental metal···metal distance to the sum of the metallic radii of the two metal atoms given by Pauling.[17] Formal shortness ratios ≤1.22 suggest the presence of covalent metal−metal bonding,[18] and for **1-Ho** and **1-Er**, the values are 1.183 and 1.177.

The $Ln-Cp_{cent}$ distances in **1-Ho** and **1-Er** are 2.333(1) and 2.313(1) Å, respectively. Across the $(Cp^{iPr5})_2Ln_2I_3$ series (Ln = Gd, Tb, Dy, Ho, Er), the $Ln-Cp_{cent}$ distance decreases monotonically from Gd to Er (Table S3), which is consistent with the expected trend based on the lanthanide contraction and indicates that the Ln−Cp interaction is predominantly electrostatic.[19] While the Ln−Ln distance also decreases from $(Cp^{iPr5})_2Gd_2I_3$ (3.769(1) Å) to $(Cp^{iPr5})_2Dy_2I_3$ (3.713(1) Å), this distance increases in **1-Ho** (3.740(1) Å) before decreasing again for **1-Er** (3.720(1) Å) (Figure 1c and Table S3). Previously, we performed CASSCF and density functional theory calculations on $(Cp^{iPr5})_2Ln_2I_3$ (Ln = Y, Tb, Dy) that revealed the singly occupied σ-bonding orbital originates

https://doi.org/10.1021/jacs.4c06250
J. Am. Chem. Soc. 2024, 146, 18714−18721

predominantly from the $5d_{z^2}$ ($4d_{z^2}$) orbital on each lanthanide (yttrium).[16] Consistent with these results, CASSCF calculations performed on **1-Ho** and **1-Er** (Figure 1b, see Section 9 of the Supporting Information for details) indicate that the greatest contribution to the bonding interaction is the $5d_{z^2}$ orbital on each lanthanide. Upon progressing from Gd to Er in the $(Cp^{iPr5})_2Ln_2I_3$ series, the $5d_{z^2}$ contribution decreases monotonically from 71.6 to 67.6%. For all compounds, there are also smaller contributions from the 6s and $6p_z$ orbitals on each lanthanide (Figure S36). While the 6s contribution increases monotonically from Gd to Er (from 3.9 to 5.5%), the $6p_z$ orbital contribution first increases from Gd to Dy (from 3.1 to 4.4%) and then decreases from Dy to Ho (from 4.4 to 3.0%). Interestingly, CAS(n,7)SCF calculations on the high-spin ground term of each free Ln^{III} ion in the gas phase indicate that the 6p orbitals decrease in energy from Gd^{III} to Dy^{III}, but then increase for Ho^{III} (Figure S37). Of note, a similar trend has been reported based on experimental atomic spectra for the lanthanides, where the $4f^n6s^2$ to $4f^{(n-1)}6s^26p^1$ and $4f^n$ to $4f^{(n-1)}6p^1$ excitations in Ln^0 and Ln^{II}, respectively, peak for $n = 10$ (see Figure S38).[20,21] In tandem with the overall decreasing contribution from the $5d_{z^2}$ orbitals to the σ bond in **1-Ln**, such an increase in the 6p orbital energy would lead to a decrease in overall atomic orbital contributions to the σ bond, and consequently a weaker and longer bond, consistent with the crystal structures.

UV−vis−NIR spectra collected for solutions of **1-Ho** and **1-Er** in *n*-hexanes display features associated with σ-to-π transitions below 400 nm and strong absorption ($\varepsilon \geq 11{,}000$ M^{-1} cm^{-1}) associated with σ-to-σ^* transition at higher wavelengths (Figures S9−S12). These results are again consistent with spectra reported previously for Dy and Tb analogues and further support the existence of Ln−Ln bonding interactions in **1-Ho** and **1-Er**. Diffuse reflectance spectra collected for powder samples of these **1-Ln** compounds all exhibit similar features in the visible region (Figures S13 and S14).

Magnetic Properties. Variable-temperature zero-field cooled dc magnetic susceptibility data were collected for **1-Ho** and **1-Er** between 2 and 300 K under an applied field of 1000 Oe. Corresponding molar magnetic susceptibility times temperature ($\chi_M T$) versus T data for both compounds are shown in Figure 2. At 300 K, the $\chi_M T$ values are 47.01 and 37.78 emu K/mol for **1-Ho** and **1-Er**, respectively, significantly higher than the values predicted for noninteracting Ln^{III} ($4f^n$) and Ln^{II} ($4f^n5d^1$) ions (30.97 and 25.54 emu K/mol, respectively, within the $L-S$ coupling model[14]). As the temperature is lowered from 300 K, $\chi_M T$ reaches a maximum value of 55.94 emu K/mol for **1-Ho** and 42.40 emu K/mol for **1-Er** at 110 and 80 K, respectively. These values are close to the theoretical values predicted for parallel alignment of the lanthanide $4f^n$ electrons with one unpaired σ-bonding electron (58.47 and 48.04 emu K/mol, respectively). For **1-Ho**, dc magnetic susceptibility data collected after cooling under an applied field of 1 T clearly diverge from the zero-field cooled data at 28 K (Figure 2, inset), which is indicative of magnetic blocking below this temperature. In contrast, field-cooled and zero-field cooled data collected for **1-Er** overlay with one another, confirming the absence of magnetic blocking (Figure S17).

Ac magnetic susceptibility data collected for **1-Ho** under zero dc field and temperatures between 33 and 48 K revealed a frequency-dependent peak in the molar out-of-phase susceptibility (χ_M'') and a simultaneous decrease in the molar in-phase susceptibility (χ_M'), confirming magnetic blocking on a millisecond-to-second time scale (Figure 3; see Section 6 of the Supporting Information for details). The relaxation time, τ, at each temperature was extracted by fitting the corresponding plots of χ_M' and χ_M'' using a generalized Debye model (Figures S18, S19 and Table S4).[22,23] Lower-temperature relaxation times were extracted from dc relaxation data collected between 23.5 and 26 K, by fitting the time-dependent decay of the magnetization to an exponential function (see Figure S20, Table S5, and Section 6 of the Supporting Information). The combined ac and dc relaxation times were used to generate the plot of $\ln(\tau)$ versus $1/T$ shown in Figure 3b.[23] The ac relaxation data (blue data points) are linear, consistent with an Orbach relaxation process, and could be fit using the Arrhenius equation $\ln(\tau) = \ln(\tau_0) + U_{eff}(k_BT)^{-1}$ to extract a barrier to magnetic relaxation of $U_{eff} = 556(4)$ cm^{-1} and $\tau_0 = 2.4(6) \times 10^{-11}$ s; from these data, we also calculated $T_b = 27.5(2)$ K. Notably, this relaxation barrier is among the highest reported for any holmium-based single-molecule magnet,[24−28] surpassed only marginally by the value of $U_{eff} = 577(6)$ cm^{-1} reported for $[Ho^{III}Ni_5^{II}(quinha)_5F_2(dfpy)_{10}](ClO_4)\cdot 2EtOH$ (H_2quinha = quinaldic hydroxamic acid; dfpy = 3,5-difluoropyridine) (Table S6).[28]

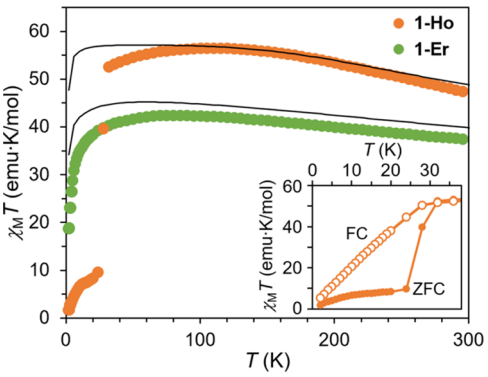

Figure 2. Temperature dependence of the static magnetic susceptibility−temperature product ($\chi_M T$) for **1-Ho** (orange) and **1-Er** (green). Magnetic susceptibility data were collected under an applied field of 1000 Oe. Black solid lines represent the calculated data obtained using full model Hamiltonian from projected CASSCF-SO parameters with exchange terms downscaled by 50% for **1-Ho** and 20% for **1-Er**, as described in the text. Inset: field-cooled (FC) and zero-field-cooled (ZFC) magnetic susceptibility data for **1-Ho** under an applied field of 1000 Oe.

Variable-field magnetization data collected for **1-Ho** by first cooling the sample under zero field and then sweeping the field between +7 and −7 T revealed open magnetic hysteresis at temperatures as high as 30 K (Figure S22). At 7 T, the magnetization reached 11.3 μ_B, higher than the predicted spin-only moment of 9 μ_B for two Ho^{III} ($4f^{10}$) ions and one unpaired electron, as a result of orbital angular momentum contributions from the 4f electrons. Additional data were collected after magnetizing the sample at 100 K using a 7 T field, cooling to 21, 23, 24, or 25 K, and then sweeping the field from +7 to −7 T (Figure S23). At 7 T and 21 K, the sample magnetization was 11.9 μ_B, slightly higher than that achieved when the sample was cooled under zero field, indicating that the magnetization is not saturated by a 7 T field. From these demagnetization data, we estimate a lower bound for the coercive field of $H_c > 7$ T for temperatures ≤21 K.

https://doi.org/10.1021/jacs.4c06250
J. Am. Chem. Soc. 2024, 146, 18714−18721

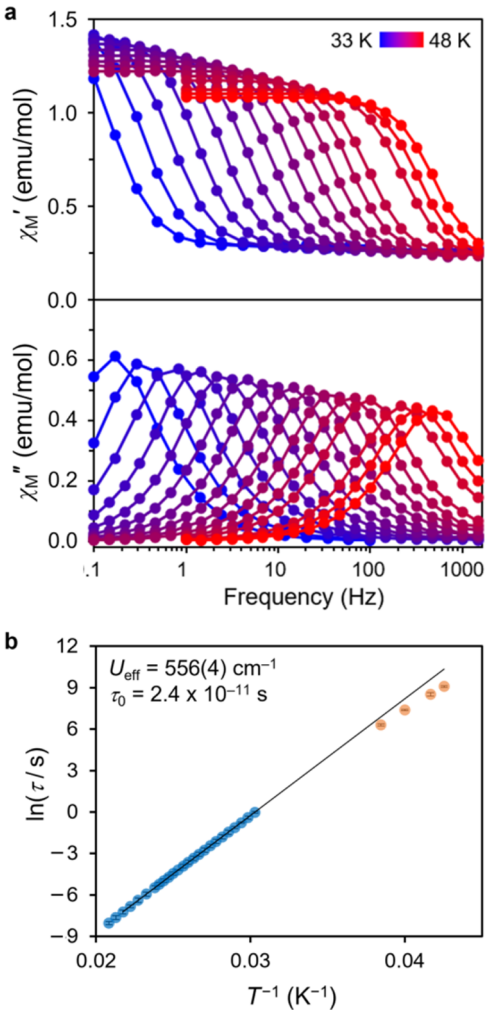

Figure 3. (a) Plot of in-phase (χ_M') and out-of-phase (χ_M'') molar magnetic susceptibility collected for **1-Ho** from 33 to 48 K under zero applied field. (b) Plot of the natural log of the relaxation time versus $1/T$ for **1-Ho**. Blue circles represent data extracted from fitting the χ_M' and χ_M'' data using a generalized Debye model. Yellow circles represent data extracted from fitting dc relaxation data (see Section 6 of the Supporting Information for details). The black line represents a fit to the Arrhenius equation. The $\tau_{\pm}$ (1σ) uncertainty ranges for each τ value are indicated with error bars (see Tables S4 and S5).[23]

Variable-field magnetization data were also collected for **1-Ho** at 20 K and magnetic fields between +35 and −35 T (Figure 4). It was possible to fully saturate **1-Ho** at these higher fields, revealing a saturation magnetization of M_s = 13.5 μ_B and H_c = 20.1 T (Figures 4, red trace and S24). The coercive field was also measured at even lower temperatures, by first magnetizing the sample at 35 T and 100 K, cooling to the desired temperature, and then sweeping the field to −35 T. From these data, we found H_c = 27 T at 16 K (Figure 4, purple trace) and H_c = 32.6 T at 8 K (Figure 4, blue trace) and 5.3 K (Figure S26), values that vastly exceed the coercivities of the commercial magnets $SmCo_5$ (4.3 T at 4.2 K) and $Nd_2Fe_{14}B$ (5.0 T at 80 K).[29]

Electronic Structure and Magnetic Coupling. The starkly different magnetic properties of **1-Ho** and **1-Er** are consistent with predictions from the simple qualitative model previously developed for guiding lanthanide single-molecule magnet design.[5] In particular, the axial crystal field experienced

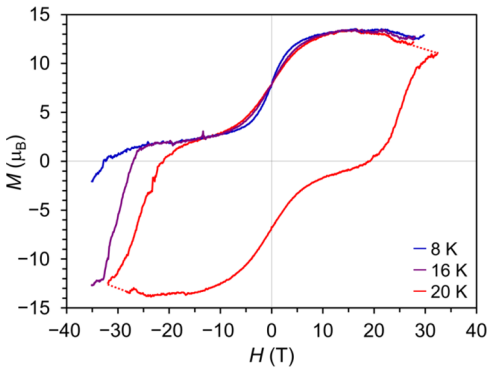

Figure 4. Variable-field magnetization data obtained for **1-Ho** between ±35 T at 20 K (red) overlaid with field-cooled magnetization data collected at 16 K (purple) and 8 K (blue), as described in the text. All data were collected using a sweep rate of 1.7 kOe/s. The dotted lines in the 20 K data are guides for the eye; the measured values in these regions showed an anomalous jump (see Figure S25), which is an artifact likely due to sample movement at such high fields.

by the lanthanide ions in these compounds should stabilize M_J states with oblate electron densities, such as the maximal M_J states for Ho^{III}, and destabilize M_J states that are more prolate in character, such as the maximal M_J states of Er^{III} (see Figure S39a for a qualitative illustration of this concept, and the reader is referred to a detailed discussion of these points in ref 5). CASSCF-SO calculations were carried out on **1-Ho** and **1-Er** to quantitatively evaluate differences in their electronic structures and magnetic anisotropies (see Section 9 of the Supporting Information for full details).

Consistent with results obtained previously for $(Cp^{iPr5})_2Ln_2I_3$ (Ln = Tb, Dy), both **1-Ho** and **1-Er** feature a one-electron metal−metal σ bond that is predominantly of $5d_{z^2}$ parentage (Figures 1b, S28, and S29). To separate the different effects arising from the crystal field, spin−orbit coupling, and exchange interactions, we adopted the following approach based on our prior work.[16,30] First, from a CASSCF calculation of the high-spin ground state of the full molecule, we froze the σ-bonding orbital; we then substituted one Ln^{III} center with a closed-shell $4f^{14}$ Lu^{III} center and performed two CASSCF calculations for the high and low spin configurations of the remaining open-shell Ln^{III} center interacting with the σ electron. Finally, we mixed these states with spin−orbit coupling and projected the *ab initio* Hamiltonian onto a model Hamiltonian describing each of the crystal field, spin−orbit, and exchange interactions uniquely, and this calculation was repeated for the other Ln^{III} centers (see Tables S7 and S8; note that the z-axis is defined as the Ln−Ln axis).

For **1-Ho**, the single-ion anisotropy arising from the combined crystal field of the Cp^{iPr5} ligand and the coaxial σ electron (without the 4f−σ spin−spin coupling; Table S9) is easy-axis type, stabilizing a mixed 86%|±7> + 12%|±8> ground pseudodoublet (g_z = 17.9) for each ion. Of note, this ground state is not the maximal M_J = ±8, and it is significantly more mixed than the single-ion ground states calculated for $(Cp^{iPr5})_2Tb_2I_3$ and $(Cp^{iPr5})_2Dy_2I_3$, and is separated from the first excited (pseudo)doublet (87%|±8> + 12%|±7>) state by only 46 cm^{-1}, compared to corresponding energy gaps of more than 200 cm^{-1} calculated for the Tb and Dy variants.[16] The calculated 4f−σ spin−spin coupling in **1-Ho** is dominated by the isotropic spin−spin term, with a value of approximately +1960 cm^{-1}, corresponding to $J_{4f-\sigma}$ = +490 cm^{-1} for a $-2J$

https://doi.org/10.1021/jacs.4c06250
J. Am. Chem. Soc. 2024, 146, 18714−18721

Heisenberg Hamiltonian (Table S7). This value is comparable to those obtained from similar calculations on $(Cp^{iPr5})_2Tb_2I_3$ ($J_{4f-\sigma}$ = +519 cm^{-1}) and $(Cp^{iPr5})_2Dy_2I_3$ ($J_{4f-\sigma}$ = +524 cm^{-1}).[16]

Using the projected parameters for both Ln^{III} centers to build a model Hamiltonian for the complete molecule, we found that **1-Ho** has a majority M_J = ±33/2 ground state arising from the $^{10}Q_{33/2}$ multiplet (see Figure S39b, S = 9/2, L = 12, J = 33/2), corresponding to parallel alignment of all angular momenta, with a majority M_J = ±31/2 first excited state at 87 cm^{-1} (see Figure S30 and Table S10). Using this model Hamiltonian to calculate the magnetic susceptibility, the low-temperature maximum was well-reproduced. We note, however, that the high-temperature slope is too flat (Figure S31), implying that the 4f−σ exchange is overpredicted by CASSCF-SO, just as was previously found for **1-Gd**.[16] Indeed, the CASSCF-SO-based model predicts two doublets with small angular momentum (i.e., through which magnetic relaxation can readily proceed) at 938 and 939 cm^{-1} (Table S10), which are substantially higher in energy than the experimental relaxation barrier of U_{eff} = 556(4) cm^{-1}. We previously found that dynamic correlation effects could reduce the exchange coupling, and that this could be replicated simply by down-scaling the CASSCF-SO-calculated exchange parameters.[16] Downscaling all exchange terms for **1-Ho** by 50% gives a calculated high-temperature magnetic susceptibility in good agreement with experiment (Figure 2) and two doublets with small angular momentum at 503 and 510 cm^{-1}, in good agreement with the measured value of U_{eff} (see Figure 5a and Table S11). We note that a 50% downscaling is rather drastic, compared to the 20% downscaling required previously for $(Cp^{iPr5})_2Tb_2I_3$.[16] Because of this, we also performed multistate complete active space second-order perturbation theory (CASPT2) calculations (see the Supporting Information) on the two halves of **1-Ho**, which indeed reduced the isotropic spin−spin exchange coupling by approximately 60% (Table S12). However, there is a significant change in the crystal field terms and the predicted magnetic susceptibility is in poor agreement with experiment (Figure S33). Hence, CASPT2 appears not to be appropriate in this case, although it does support a large downscaling of the exchange terms arising from dynamic correlation.

Following the same approach for **1-Er**, we found that the single-ion anisotropy arising from the Cp^{iPr5} ligand and the coaxial σ electron (without 4f−σ spin−spin coupling; Table S13) stabilizes a 67%|±5/2> + 20%|±3/2> ground doublet (g_x = 12.6, g_y = 1.2, g_z = 0.9) for each Er^{III} center, which is separated by only 21 cm^{-1} from the first excited pseudodoublet (40%|±7/2> + 25%|±3/2> + 22%|±5/2>). The CASSCF-SO-calculated 4f−σ exchange coupling is again dominated by the isotropic spin−spin term with a value of approximately +1380 cm^{-1}, which corresponds to $J_{4f-\sigma}$ = +460 cm^{-1} for a −2J Heisenberg Hamiltonian (Table S8). Building a model Hamiltonian for the complete molecule revealed a ground $^8Q_{31/2}$ multiplet (S = 7/2, L = 12, J = 31/2; Table S14), corresponding to parallel alignment of all angular momenta, as found for **1-Ho**. However, as the single-ion anisotropy is of strong easy-plane type, the resulting crystal field states are inverted compared to those of **1-Ho** (Figure S34) and consist of very mixed doublets, e.g., the ground doublet is 50%|$^8Q_{31/2}$, ±11/2> + 15%|$^8Q_{31/2}$, ±9/2> + 12%|$^8Q_{31/2}$, ±13/2> with a first excited state (34%|$^8Q_{31/2}$, ±13/2> + 23%|$^8Q_{31/2}$, ±9/2> + 17%|$^8Q_{31/2}$, ±11/2>) at ∼1 cm^{-1}. Such an electronic spectrum would not be expected to give rise to any single-molecule magnet behavior, in agreement with experimental magnetic data for **1-Er**. Calculated magnetic susceptibility data obtained with the model Hamiltonian and the exchange terms downscaled by 20% are in good agreement with the experimental data (Figure 2).

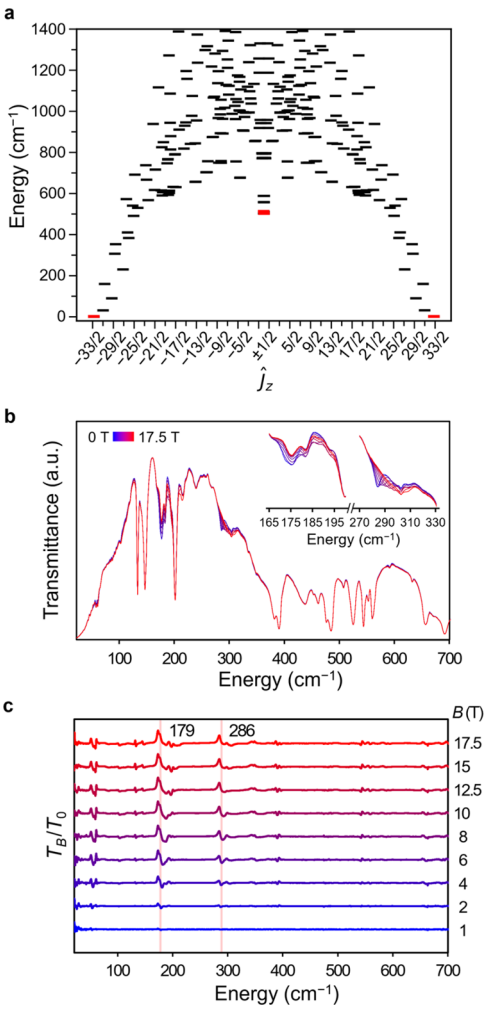

Figure 5. (a) Ground state splitting calculated for **1-Ho** from the full model Hamiltonian using projected CASSCF-SO parameters with exchange terms downscaled by 50%. States given in a 0.01 T field along z to quantize the M_J projection. (b) Transmission spectra for **1-Ho** collected at 4.2 K under applied fields ranging from 0 to 17.5 T. (c) Plots of applied-field spectra (T_B) divided by the zero-field spectrum (T_0), where B is the applied field. The spectra have been offset vertically for better visual clarity.

Far-Infrared Magnetospectroscopy (FIRMS). To probe the calculated ground-state splitting for **1-Ho** and **1-Er** experimentally, we analyzed both compounds using far-infrared magnetospectroscopy (FIRMS). This technique provides a means of directly measuring the energies of magnetic microstates, and can be used to validate experimental U_{eff} values for systems where relaxation occurs between the ground and low-lying excited states.[31] Two types of field-dependent transitions can be observed: purely electronic transitions, governed by the magnetic dipole selection rule ΔM_J = 0, ±1,[31,32] and mixed vibronic transitions, involving a simultaneous change in both electronic and vibrational states due to spin-phonon coupling.[33] Here, we focused on analysis of the magnetic dipole transitions between M_J sublevels.

https://doi.org/10.1021/jacs.4c06250
J. Am. Chem. Soc. 2024, 146, 18714−18721

Transmission spectra were collected on microcrystalline powder samples of **1-Ho** and **1-Er** between 20 and 700 cm^{-1} at 5.5 K under applied fields ranging from 0 to 17.5 T (see Figures 5b and S27a). To discern magnetic dipole transitions from field-independent signals originating from molecular vibrations and instrument response, we divided the spectra collected under applied fields by the corresponding zero-field spectrum for each compound, to arrive at the normalized spectra shown in Figures 5c and S27b. For **1-Ho**, these spectra feature clear field-dependent signals at transition energies of 179 and 286 cm^{-1} (Figure 5c). Using the model Hamiltonian described above (including 50% downscaling of exchange terms), we calculated all the magnetic dipole transitions for **1-Ho** in this energy range (Figure S32). The two strongest transitions occur at 231 and 307 cm^{-1} (Figure S32; corresponding to the transitions 90%$|^{10}Q_{33/2}, \pm 33/2\rangle \rightarrow$ 76%$|^{10}Q_{33/2}, \pm 27/2\rangle$ and 90%$|^{10}Q_{33/2}, \pm 33/2\rangle \rightarrow$ 64%$|^{10}O_{31/2}, \pm 29/2\rangle$ + 21%$|^{8}Q_{31/2}, \pm 29/2\rangle$, respectively), in reasonable agreement with the experimental data. On the other hand, the corresponding spectra collected for **1-Er** feature multiple field-dependent signals over a broad range of energies <150 cm^{-1} (Figure S27), indicating the existence of multiple low-lying magnetic microstates such as those predicted from our computational results (Figure S34).

CONCLUSIONS

Two new mixed-valence dilanthanide complexes, $(Cp^{iPr5})_2Ho_2I_3$ (**1-Ho**) and $(Cp^{iPr5})_2Er_2I_3$ (**1-Er**), were synthesized and characterized for comparison with the first, previously reported complexes of this type $(Cp^{iPr5})_2Ln_2I_3$ (Ln = Y, Gd, Tb, Dy).[16] Structural and spectroscopic data are consistent with the presence of lanthanide−lanthanide bonding in **1-Ho** and **1-Er**, while CASSCF calculations indicate that the bonding interactions arise from a singly occupied σ-type bonding orbital that is predominantly $5d_{z^2}$ in character, as also found previously for the Gd, Tb, and Dy complexes. Interestingly, in comparing the series of complexes, while the Ln−Ln distance steadily decreases from Gd to Dy, consistent with the expected decrease in ionic radii, it increases again in the Ho and Er variants, which computations suggest is due to a decrease in the 6p orbital contribution to bonding. Static and dynamic magnetic susceptibility data collected for **1-Ho** revealed that this compound exhibits a record blocking temperature of 27.5 K among holmium single-molecule magnets and an exceedingly large magnetic coercivity ($H_c \geq$ 32.6 T at 8 K) that surpasses that of commercial bulk magnets. In contrast, **1-Er** does not behave as a single-molecule magnet. These results are consistent with the well-established qualitative crystal field model for optimizing lanthanide single-ion anisotropies, which predicts that axial ligand fields will stabilize maximal M_J states that are oblate in character, such as those of Ho^{III}, and destabilize maximal M_J states that are prolate in character, such as those for Er^{III}. CASSCF-SO calculations, supported by FIRMS data, reveal that the strong axial crystal field in these compounds favors a maximal total angular momentum ground state for **1-Ho**, whereas the ground state for **1-Er** is nonmaximal and highly mixed. Ultimately, the results here for **1-Ho** are significant, as Ho^{III} single-molecule magnets with large coercivities have previously been elusive, due in large part to the fact that Ho^{III} is a non-Kramers ion with lower anisotropy in its 4f shell than Tb^{III} or Dy^{III}.[5] Our results highlight that by harnessing Ln−Ln bonding interactions within an appropriate ligand field, it is possible to design new high-performance single-molecule magnets even with previously seemingly intractable lanthanide ions.

ASSOCIATED CONTENT

Supporting Information

The Supporting Information is available free of charge at https://pubs.acs.org/doi/10.1021/jacs.4c06250.

The synthesis, X-ray crystallographic analysis, and FT-IR spectra for all compounds; UV−vis-NIR spectra; and additional experimental details for DC and AC magnetic susceptibility measurements, DC magnetic relaxation measurements, variable field magnetization measurements, far-infrared magnetospectroscopy, and computations (PDF)

Accession Codes

CCDC 2353942−2353945 contain the supplementary crystallographic data for this paper. These data can be obtained free of charge via www.ccdc.cam.ac.uk/data_request/cif, or by emailing data_request@ccdc.cam.ac.uk, or by contacting The Cambridge Crystallographic Data Centre, 12 Union Road, Cambridge CB2 1EZ, U.K.; fax: +44 1223 336033.

AUTHOR INFORMATION

Corresponding Authors

K. Randall McClain − *US Navy, Naval Air Warfare Center, Weapons Division, Research Department, Chemistry Division, China Lake, California 93555, United States;* orcid.org/0000-0001-8072-8402; Email: kenneth.r.mcclain7.civ@us.navy.mil

Eun Sang Choi − *National High Magnetic Field Laboratory, Florida State University, Tallahassee, Florida 32310, United States*; Email: echoi@magnet.fsu.edu

Nicholas F. Chilton − *Department of Chemistry, The University of Manchester, Manchester M13 9PL, U.K.; Research School of Chemistry, The Australian National University, Canberra, ACT 2601, Australia;* orcid.org/0000-0002-8604-0171; Email: nicholas.chilton@anu.edu.au

Jeffrey R. Long − *Department of Chemistry, Department of Chemical and Biomolecular Engineering, and Department of Materials Science and Engineering, University of California, Berkeley, Berkeley, California 94720, United States; Materials Sciences Division, Lawrence Berkeley National Laboratory, Berkeley, California 94720, United States;* orcid.org/0000-0002-5324-1321; Email: jrlong@berkeley.edu

Authors

Hyunchul Kwon − *Department of Chemistry, University of California, Berkeley, Berkeley, California 94720, United States*

Jon G. C. Kragskow − *Department of Chemistry, The University of Manchester, Manchester M13 9PL, U.K.*

Jakob K. Staab − *Department of Chemistry, The University of Manchester, Manchester M13 9PL, U.K.*

Mykhaylo Ozerov − *National High Magnetic Field Laboratory, Florida State University, Tallahassee, Florida 32310, United States;* orcid.org/0000-0002-5470-1158

Katie R. Meihaus − *Department of Chemistry, University of California, Berkeley, Berkeley, California 94720, United States*

Benjamin G. Harvey − *US Navy, Naval Air Warfare Center, Weapons Division, Research Department, Chemistry Division, China Lake, California 93555, United States;* orcid.org/0000-0003-2091-3539

Complete contact information is available at: https://pubs.acs.org/10.1021/jacs.4c06250

Author Contributions

◆H.K. and K.R.M. contributed equally.

Notes

The authors declare no competing financial interest.

■ ACKNOWLEDGMENTS

This research was supported by NSF grant CHE-2102603. Additional support was provided by the Naval Air Warfare Center Weapons Division NISE program (K.R.M. and B.G.H.), ERC grant STG-851504 (J.G.C.K., J.K.S., and N.F.C.), and Royal Society URF191320 (N.F.C.), and Leverhulme Trust RPG-2023-025 (N.F.C.). A portion of this work was performed at the National High Magnetic Field Laboratory, which is supported by National Science Foundation Cooperative Agreement No. DMR-1644779 and DMR-2128556 and the State of Florida. We thank the University of Manchester for access to the Computational Shared Facility, the ILJU Academy and Culture Foundation for support of H.K. through an Overseas Ph.D. Scholarship, and Dr. T. David Harris for discussions and editorial assistance.

■ REFERENCES

(1) Gatteschi, D.; Sessoli, R.; Villain, J.Single-Molecule Magnets. In *Molecular Nanomagnets*, 2006; Vol. *1*, pp 108−159.

(2) Chilton, N. F. Molecular Magnetism. *Annu. Rev. Mater. Res.* **2022**, *52*, 79−101.

(3) Ishikawa, N.; Sugita, M.; Ishikawa, T.; Koshihara, S.; Kaizu, Y. Mononuclear Lanthanide Complexes with a Long Magnetization Relaxation Time at High Temperatures: A New Category of Magnets at the Single-Molecular Level. *J. Phys. Chem. B* **2004**, *108* (31), 11265−11271.

(4) Tang, J.; Zhang, P. *Lanthanide Single Molecule Magnets*; Springer Berlin, Heidelberg, 2015.

(5) Rinehart, J. D.; Long, J. R. Exploiting Single-Ion Anisotropy in the Design of f-Element Single-Molecule Magnets. *Chem. Sci.* **2011**, *2* (11), 2078.

(6) Goodwin, C. A. P.; Ortu, F.; Reta, D.; Chilton, N. F.; Mills, D. P. Molecular Magnetic Hysteresis at 60 Kelvin in Dysprosocenium. *Nature* **2017**, *548* (7668), 439−442.

(7) Guo, F.-S.; Day, B. M.; Chen, Y.-C.; Tong, M.-L.; Mansikkamäki, A.; Layfield, R. A. Magnetic Hysteresis up to 80 Kelvin in a Dysprosium Metallocene Single-Molecule Magnet. *Science* **2018**, *362* (6421), 1400−1403.

(8) Ungur, L.; Le Roy, J. J.; Korobkov, I.; Murugesu, M.; Chibotaru, L. F. Fine-tuning the Local Symmetry to Attain Record Blocking Temperature and Magnetic Remanence in a Single-Ion Magnet. *Angew. Chem., Int. Ed.* **2014**, *53* (17), 4413−4417.

(9) Münzfeld, L.; Schoo, C.; Bestgen, S.; Moreno-Pineda, E.; Köppe, R.; Ruben, M.; Roesky, P. W. Synthesis, Structures and Magnetic Properties of $[(h^9\text{-}C_9H_9)Ln(h^8\text{-}C_8H_8)]$ Super Sandwich Complexes. *Nat. Commun.* **2019**, *10* (1), No. 3135.

(10) McClain, K. R.; Gould, C. A.; Chakarawet, K.; Teat, S. J.; Groshens, T. J.; Long, J. R.; Harvey, B. G. High-Temperature Magnetic Blocking and Magneto-Structural Correlations in a Series of Dysprosium(III) Metallocenium Single-Molecule Magnets. *Chem. Sci.* **2018**, *9* (45), 8492−8503.

(11) MacDonald, M. R.; Bates, J. E.; Ziller, J. W.; Furche, F.; Evans, W. J. Completing the Series of + 2 Ions for the Lanthanide Elements: Synthesis of Molecular Complexes of Pr^{2+}, Gd^{2+}, Tb^{2+}, and Lu^{2+}. *J. Am. Chem. Soc.* **2013**, *135* (26), 9857−9868.

(12) Meihaus, K. R.; Fieser, M. E.; Corbey, J. F.; Evans, W. J.; Long, J. R. Record High Single-Ion Magnetic Moments Through $4f^n$ $5d^1$ Electron Configurations in the Divalent Lanthanide Complexes $[(C_5H_4SiMe_3)_3Ln]^-$. *J. Am. Chem. Soc.* **2015**, *137* (31), 9855−9860.

(13) Evans, W. J.; Walensky, J. R.; Furche, F.; DiPasquale, A. G.; Rheingold, A. L. Trigonal-Planar versus Pyramidal Geometries in the Tris(Ring) Heteroleptic Divalent Lanthanide Complexes (C_5Me_5)-$Ln(\mu\text{-}\eta^6:\eta^1\text{-}Ph)_2BPh_2$: Crystallographic and Density Functional Theory Analysis. *Organometallics* **2009**, *28* (20), 6073−6078.

(14) McClain, K. R.; Gould, C. A.; Marchiori, D. A.; Kwon, H.; Nguyen, T. T.; Rosenkoetter, K. E.; Kuzmina, D.; Tuna, F.; Britt, R. D.; Long, J. R.; Harvey, B. G. Divalent Lanthanide Metallocene Complexes with a Linear Coordination Geometry and Pronounced 6s−5d Orbital Mixing. *J. Am. Chem. Soc.* **2022**, *144* (48), 22193−22201.

(15) Gould, C. A.; McClain, K. R.; Yu, J. M.; Groshens, T. J.; Furche, F.; Harvey, B. G.; Long, J. R. Synthesis and Magnetism of Neutral, Linear Metallocene Complexes of Terbium(II) and Dysprosium(II). *J. Am. Chem. Soc.* **2019**, *141* (33), 12967−12973.

(16) Gould, C. A.; McClain, K. R.; Reta, D.; Kragskow, J. G. C.; Marchiori, D. A.; Lachman, E.; Choi, E.-S.; Analytis, J. G.; Britt, R. D.; Chilton, N. F.; Harvey, B. G.; Long, J. R. Ultrahard Magnetism from Mixed-Valence Dilanthanide Complexes with Metal-Metal Bonding. *Science* **2022**, *375* (6577), 198−202.

(17) Pauling, L. *The Nature of the Chemical Bond*, 3rd ed.; Cornell University Press, 1960; pp 400−404.

(18) Chipman, J. A.; Berry, J. F. Paramagnetic Metal-Metal Bonded Heterometallic Complexes. *Inorg. Chem.* **2023**, *62* (9), 3715−3721.

(19) Jordan, R. B. Lanthanide Contraction: What Is Normal? *Inorg. Chem.* **2023**, *62* (9), 3715−3721.

(20) Martin, W. C.; Zalubas, R.; Hagan, L. Atomic Energy Levels − The Rare-Earth Elements. *Natl. Stand. Ref. Data Ser.* **1978**, *60*, 422.

(21) Spector, N.; Sugar, J.; Wyart, J.-F. Analysis of the Third Spectrum of Dysprosium (Dy III). *J. Opt. Soc. Am. B* **1997**, *14* (3), 511−521.

(22) Cole, K. S.; Cole, R. H. Dispersion and Absorption in Dielectrics I. Alternating Current Characteristics. *J. Chem. Phys.* **1941**, *9* (4), 341−351.

(23) Reta, D.; Chilton, N. F. Uncertainty Estimates for Magnetic Relaxation Times and Magnetic Relaxation Parameters. *Phys. Chem. Chem. Phys.* **2019**, *21* (42), 23567−23575.

(24) Blagg, R. J.; Tuna, F.; McInnes, E. J. L.; Winpenny, R. E. P. Pentametallic Lanthanide-Alkoxide Square-Based Pyramids: High Energy Barrier for Thermal Relaxation in a Holmium Single Molecule Magnet. *Chem. Commun.* **2011**, *47* (38), 10587.

(25) Chen, Y.-C.; Liu, J.-L.; Wernsdorfer, W.; Liu, D.; Chibotaru, L. F.; Chen, X.-M.; Tong, M.-L. Hyperfine-Interaction-Driven Suppression of Quantum Tunneling at Zero Field in a Holmium(III) Single-Ion Magnet. *Angew. Chem., Int. Ed.* **2017**, *56* (18), 4996−5000.

(26) Kajiwara, T. A Holmium(III)-Based Single-Molecule Magnet with Pentagonal-Bipyramidal Geometry. *Angew. Chem., Int. Ed.* **2017**, *56* (38), 11306−11308.

(27) Ma, Y.; Zhai, Y.-Q.; Ding, Y.-S.; Han, T.; Zheng, Y.-Z. Understanding a Pentagonal-Bipyramidal Holmium(III) Complex with a Record Energy Barrier for Magnetisation Reversal. *Chem. Commun.* **2020**, *56* (28), 3979−3982.

(28) Wu, S.-G.; Ruan, Z.-Y.; Huang, G.-Z.; Zheng, J.-Y.; Vieru, V.; Taran, G.; Wang, J.; Chen, Y.-C.; Liu, J.-L.; Ho, L. T. A.; Chibotaru, L. F.; Wernsdorfer, W.; Chen, X.-M.; Tong, M.-L. Field-Induced Oscillation of Magnetization Blocking Barrier in a Holmium Metallacrown Single-Molecule Magnet. *Chem* **2021**, *7* (4), 982−992.

(29) Kütterer, R.; Hilzinger, H.-R.; Kronmüller, H. The Temperature Dependence of the Coercive Field of Co_5Sm Magnets. *J. Magn. Magn. Mater.* **1977**, *4* (1−4), 1−7.

(30) Zhang, P.; Nabi, R.; Staab, J. K.; Chilton, N. F.; Demir, S. Taming Super-Reduced Bi_2^{3-} Radicals with Rare Earth Cations. *J. Am. Chem. Soc.* **2023**, *145* (16), 9152−9163.

(31) Bunting, P. C.; Atanasov, M.; Damgaard-Møller, E.; Perfetti, M.; Crassee, I.; Orlita, M.; Overgaard, J.; Van Slageren, J.; Neese, F.; Long, J. R. A Linear Cobalt(II) Complex with Maximal Orbital Angular Momentum from a Non-Aufbau Ground State. *Science* **2018**, *362* (6421), No. eaat7319.
(32) Moreno Pineda, E.; Chilton, N. F.; Marx, R.; Dörfel, M.; Sells, D. O.; Neugebauer, P.; Jiang, S.-D.; Collison, D.; Van Slageren, J.; McInnes, E. J. L.; Winpenny, R. E. P. Direct Measurement of Dysprosium(III)dysprosium(III) Interactions in a Single-Molecule Magnet. *Nat. Commun.* **2014**, *5* (1), No. 5243.
(33) Kragskow, J. G. C.; Marbey, J.; Buch, C. D.; Nehrkorn, J.; Ozerov, M.; Piligkos, S.; Hill, S.; Chilton, N. F. Analysis of Vibronic Coupling in a 4f Molecular Magnet with FIRMS. *Nat. Commun.* **2022**, *13* (1), No. 825.

https://doi.org/10.1021/jacs.4c06250
J. Am. Chem. Soc. 2024, 146, 18714−18721